# Chaos synchronization among orthogonally polarized emissions in a dual-polarization laser

Kenju Otsuka,[1] Kana Nemoto,[2] Koji Kamikariya,[1] Yoshihiko Miyasaka,[1] Jing-Yuan Ko,[3] and Chi-Ching Lin[3]
[1]*Department of Human and Information Science, Tokai University, 1117 Kitakaname, Hiratsuka, Kanagawa, 259-1292 Japan*
[2]*Department of Physics, Tokai University, 1117 Kitakaname, Hiratsuka, Kanagawa, 259-1292 Japan*
[3]*Department of Physics, National Kaohsiung Normal University, 116 Ho-Ping First Road, Kaohsiung 802, Taiwan*
(Received 13 December 2006; revised manuscript received 22 May 2007; published 6 August 2007)

We report on the experimental observations of chaos synchronizations among orthogonally polarized emissions in a dual-polarization laser. With a three-mode scheme with a single mode in one polarization and two modes in orthogonal polarizations, synchronization was achieved by the cross-saturation dynamics of population inversions when one of the dual-polarized emissions was subjected to external perturbations, i.e., self-mixing modulation or optical fiber feedback. In-phase synchronization or lag synchronization among orthogonally polarized emissions was achieved depending on the degree of cross saturation in the self-mixing modulation. Synchronization of random bursting was observed in the fiber feedback, in which two chaotic-spiking modes in one polarization with anticorrelated intensity variations synchronize the remaining mode in the orthogonal polarization cooperatively with their total intensity variation. Information sender-mediator-receiver relationships among modes, which represent the dynamical roles of individual modes for establishing the observed three types of collective synchronizations, were identified in terms of an information circulation analysis.

DOI: 10.1103/PhysRevE.76.026204 PACS number(s): 05.45.Xt, 42.55.Px, 42.55.Rz, 42.65.Sf

## I. INTRODUCTION

Mutual coupling of nonlinear oscillators sometimes results in synchronization that plays key functional roles in various physical systems. In particular, chaos synchronizations (CS) in laser systems has attracted much attention as a relevant problem in nonlinear dynamics. CS in lasers has been studied experimentally in two or three interacting lasers, and different types of chaos synchronization, such as generalized, phase, lag, and anticipating CS, have been demonstrated in gas lasers [1], solid-state lasers [2], and semiconductor laser diodes (LDs) [3]. Most recently, Fischer *et al.* demonstrated zero-lag long-range synchronization of *two* semiconductor lasers with delayed interaction by introducing a *third* LD as a dynamical relaying element. They discussed such a collective behavior, featuring scale-free synchronization [4] in relation to coupled thermoreceptor neurons [5]. Most of the CS experiments in lasers have been achieved by *coherent* coupling of lasing fields in active media, such as injection locking of lasers in various coupling schemes, except for a few examples [1,6,7]. However, such a coherent coupling may not always be essential for synchronizations in general physical and biological systems. On the other hand, dynamical behaviors such as antiphase dynamics, clustering, grouping, and cooperative synchronizations have been studied numerically in lasers oscillating in many globally coupled longitudinal modes through cross saturation of population inversions, i.e., incoherent coupling among lasing modes [8–10].

We are experimentally studying the chaos synchronization of globally coupled three-mode ($N=3$) lasers through incoherent coupling among lasing modes as a basis for understanding synchronizations in complex systems with many coupled elements, focusing on the response of the whole system to the perturbation to some of the system variables. This approach to chaos synchronization exploits the polarization degree of freedom of light, and synchronization of orthogonally polarized emissions has been achieved by cross-saturation dynamics of population inversions, i.e., crossed-polarization gain modulation in a dual-polarization laser.

The system described here has the advantage that it allows one to use a single laser source instead of three interacting lasers; furthermore, our coupling scheme seems to be easy to implement. Synchronization of all lasing modes or lag synchronization among orthogonally polarized modes was achieved in the self-mixing modulation, depending on the degree of cross saturation. A kind of cooperative chaos synchronization was found in the fiber feedback, in which two chaotic-spiking modes with anticorrelated intensity variations in one polarization synchronize the remaining mode in the orthogonal polarization cooperatively with their total intensity variation. Polarization effects have been reported in semiconductor lasers [11,12], including chaos synchronization in coupled vertical cavity surface emitting lasers (VCSELs) [13]. However, such chaos synchronization phenomena have yet to be reported. Observed synchronizations have been characterized in terms of information relationships by information circulation analysis and the dynamical roles of individual modes for synchronizations have been identified.

The paper is organized as follows. In Sec. II, fundamental dual-polarization oscillation properties of a LD-pumped thin-slice $Nd:GdVO_4$ laser, such as pump-dependent changes in modal output powers and lasing transverse patterns, are described. Synchronization behaviors among orthogonally polarized modes under two different external perturbation schemes, i.e., self-mixing modulation with a Doppler-shifted light feedback and optical feedback from a distant reflective surface of the fiber, are addressed in Sec. III. Section IV discusses dynamical characterizations of observed phenomena in terms of information circulation analysis. Section V summarizes the results.

 

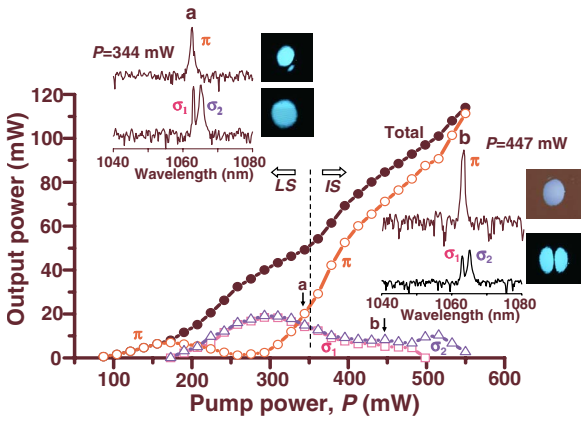


FIG. 1. (Color online) Modal and total output powers from a dual-polarized Nd:$GdVO_4$ laser as a function of pump power. Example optical spectra and their far-field patterns for $\pi$- and $\sigma$-polarized emissions are depicted.

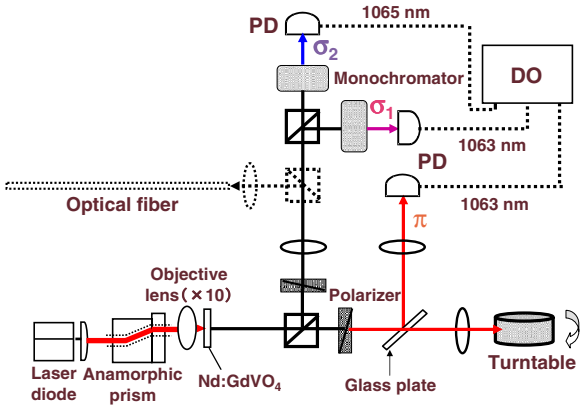


FIG. 2. (Color online) Experimental setup for cross-polarized gain modulation of a Nd:$GdVO_4$ laser. PD: photodiode, DO: digital oscilloscope.

## II. DUAL-POLARIZATION OSCILLATION IN Nd:$GdVO_4$ LASERS

We carried out an experiment with an LD-pumped thin-slice Nd:$GdVO_4$ laser. One end surface of the 5-mm square, 0.5-mm-thick 3 at. %-doped a-cut Nd:$GdVO_4$ laser was coated to be transmissive at the LD pump wavelength of 808 nm (85% transmission) and highly reflective (99.9%) in the lasing wavelength region from 1050 nm to 1070 nm. The other surface was coated to be 2% transmissive in the lasing wavelength region.

A typical example of input-output characteristics is shown in Fig. 1. The laser initially enters $\pi$-polarized oscillation at 1062.9 nm on the ${}^4F_{3/2}(2) \rightarrow {}^4I_{11/2}(1)$ transition. As the pump power is increased, $\sigma$-polarization oscillations on ${}^4F_{3/2}(2) \rightarrow {}^4I_{11/2}(2)$, and ${}^4F_{3/2}(1) \rightarrow {}^4I_{11/2}(1)$ transitions appear at 1065.1 and 1063.3 nm, respectively, reflecting the fluorescence properties of Nd:$GdVO_4$ crystals [14], where the $\pi$-polarization output is decreased. Here, the far-field pattern of $\sigma$ polarization appears at a position that is shifted from that of $\pi$ polarization, accompanied by a decrease in cross saturation of population inversions, as shown by **a** in Fig. 1. This observation suggests that the two transverse modes can be considered to be spatially separated local modes formed in a wide pump region compared with the lasing spot sizes due to the smaller lens effect at low pump power, which results in weak optical confinement for lasing fields [15]. As the pump power is increased further, the optical confinement increases through the thermal lens effect, $\pi$-polarization oscillation with a 80-$\mu$m beam spot size becomes dominant, and the output power of $\pi$-polarized mode increases again, with $\sigma$-polarization oscillation being suppressed accordingly. Here, the lasing pattern of $\sigma$-polarization becomes $TEM_{10}$ mode whose spatial overlap (i.e., cross saturation) with the $TEM_{00}$-mode pattern of $\pi$-polarization emission is small, as shown by **b** in Fig. 1, where $\sigma$-polarization emission takes place by expending the population inversions outside the $TEM_{00}$ mode profile of $\pi$-polarized emission. The three-dimensional cross saturation of population inversions in this situation has been calculated to be on the order of $10^{-3}$ [15]. In the oscillation spectra in Fig. 1, the $\pi$-polarization mode at 1062.9 nm and the $\sigma$-polarization modes at 1063.3 and 1065.1 nm are called $\pi$, $\sigma_1$, and $\sigma_2$ modes hereafter. In the high-pump power region, the $\sigma_1$ mode is suppressed: the $\pi$ and $\sigma_2$ modes survive. The input-output characteristics change depending on the pump-beam focusing condition, but the same qualitative property is obtained.

## III. EXPERIMENTAL SYNCHRONIZATION AMONG ORTHOGONALLY POLARIZED EMISSIONS AND NUMERICAL RESULTS

### A. Self-mixing modulation: in-phase synchronization and lag synchronization

Here, we describe the crossed-polarization gain modulation experiments with the present dual-polarization laser, in which one of the orthogonally polarized emissions was subjected to external perturbations to explore how the whole system would respond to perturbations through cross saturations of population inversions. The experimental setup is shown in Fig. 2. Two types of external perturbations, i.e., Doppler-shifted light feedback and optical fiber feedback, were examined. In the former case, the $\pi$-polarized output beam impinged on the surface of a rotating cylinder to induce chaotic oscillations through the highly sensitive self-mixing modulation effect in thin-slice lasers resulting from the interference between a lasing field and a coherent component of Doppler-shifted injection field [16,17], where the Doppler-shift frequency was tuned to the relaxation oscillation frequency. In the latter case, we launched two $\sigma$-polarized emissions into a 2-m-long single-mode optical fiber with 4% reflectance at the end surface, as depicted in Fig. 2. It is known that random chaotic bursting takes place in thin-slice multimode lasers when modal outputs are subjected to common external feedback from a distant reflective end, resulting from mode-partition-noise (i.e., modal frequency fluctuation) mediated dynamic instabilities [17,18]. In both cases, the dominant physical origin of chaotic dynamics themselves is a coherent effect, although a secondary effect of narrow-band Gaussian noise in a scattered light and

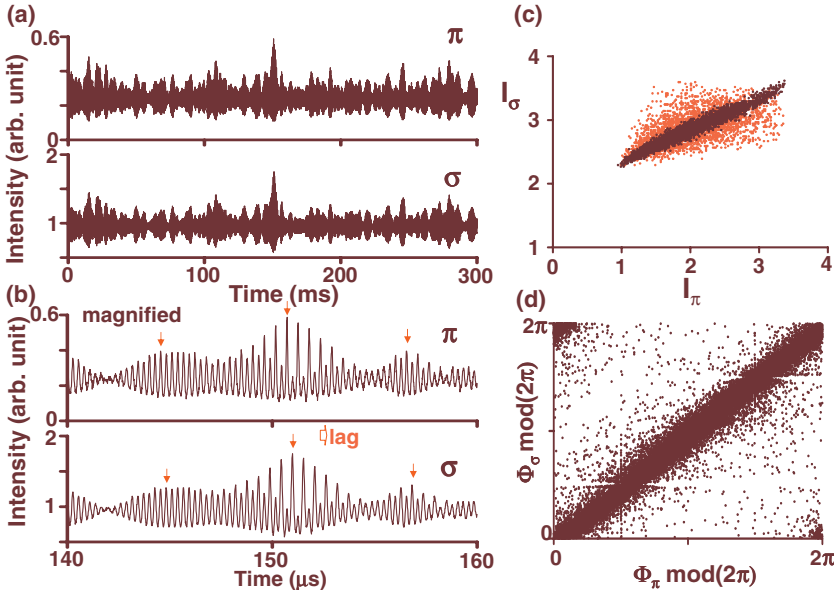


FIG. 3. (Color) Lag chaos synchronization among orthogonally polarized modes with lag time equal to the modulation period. Pump power $P=344$ mW. Modulation frequency $f_m=3.5$ MHz. (a) Intensity wave forms for $\pi$- and $\sigma$-polarized modes and (b) magnified wave forms. (c) Intensity correlation plots of experimental time series (red) and those in which the $\pi$ time series was delayed by one modulation period (black). (d) Phase correlation plots for shifted time series. The intensity correlation was fitted by $I_\sigma=0.48I_\pi+1.88$ with a standard deviation of 0.05.

phase noise are present in self-mixing and fiber feedback schemes, respectively.

As for self-mixing modulations, we found that two types of synchronizations took place among the three modes depending on the intensity ratio (i.e., degree of cross saturation) of orthogonally polarized modes, namely, lag synchronization (LS) among orthogonally polarized emissions in region **LS** and in-phase synchronization (IS) among orthogonally polarized emissions in region **IS**, as depicted in Fig. 1, in which the gradual change from LS to IS occurred with increasing pump power.

A typical intensity wave form and correlation plots for the LS state are shown in Fig. 3, where the sum of two $\sigma$ mode intensities, namely $I_\sigma$, is used for the correlation plots. In the absence of Doppler-shifted feedback, the laser exhibited only small-amplitude relaxation oscillations (less than 1% fluctuations with respect to the average power) driven by white noise. In the intensity correlation plot, we used a time series with a length of 300 $\mu$s (i.e., $5\times10^4$ data points) for each polarization output whose relative intensity was accurately calibrated from the measured output-power ratio shown in Fig. 1. Strong long-term amplitude envelope correlations are obvious in Fig. 3(a), but the time series of $I_\sigma$ is delayed as indicated by "⇒" in the magnified wave forms in Fig. 3(b). Therefore, we used the time series of $I_\pi$ delayed by a lag time (i.e., ≃one modulation period in this case; black dots) as well as the actual time series (red dots) for the intensity correlation plot [Fig. 3(c)]. As for the phase correlation plot [Fig. 3(d)], we used the Hilbert transformation to extract Gabor's analytical phase [19] from the shifted time series. This is an example of the simplest grouping of chaos states [9], in which two chaotic lasing modes in one polarization exhibit lag synchronization with the remaining orthogonally polarized chaotic lasing mode.

As the pump power was increased into the IS regime in Fig. 1, synchronizations of all lasing modes, i.e., a single mode with a $TEM_{00}$ spatial structure and two modes with $TEM_{10}$ spatial structures with fewer cross saturations, took place where mode(s) having different structures are orthogonally polarized. Typical wave forms and the corresponding intensity correlation plot for the IS state are shown in Figs. 4(a) and 4(b), respectively. It should be noted that the modulation index and envelope fluctuation amplitudes in IS state were not increased as compared with those in LS state presumably due to the increase in a rotation speed of the cylinder (modulation frequency), i.e., increased frequency broadening of a Doppler-shifted scattered light. This point will be discussed in Sec. III C.

### B. Fiber feedback: Synchronization of chaotic bursting

Random chaotic bursting in multimode thin-slice solid-state lasers coupled to a single-mode fiber, i.e., reflection from a distant reflector, has been demonstrated and reproduced numerically using the model equations including the delayed feedback and modal frequency fluctuations due to intrinsic mode partition noise [17,18]. In the present three mode oscillations, synchronized random chaotic bursting oscillations, featuring a switching between a stable (i.e., noise-driven relaxation oscillation) state and a chaotic-spiking state, were observed only when two $\sigma$ modes were subjected to the common fiber feedback in the domain of $I_\pi<I_\sigma$, i.e., 200 mW$\leqslant P\leqslant$300 mW. The synchronization was not attained when a single $\pi$ mode was subjected to the fiber feedback. On the other hand, phase synchronization in chaotic bursting has also been reported in two $CO_2$ lasers with loss modulation, partly due to an external driving and partly due to the coupling, in which bursts appear randomly as trains of large amplitude spikes intercalated by a small-amplitude chaotic regime which is not a noise-driven relaxation oscillation [20].

A typical example result of synchronized bursting in the present dual-polarization laser is shown in Figs. 4(c) and 4(d). Surprisingly, strong intensity correlation was established among detailed spiking oscillations of orthogonally polarized emissions, i.e., $I_\sigma$ and $I_\pi$. On the other hand, only phase synchronization occurs with anti-correlated intensity fluctuations among perturbed modes similar to coupled $CO_2$

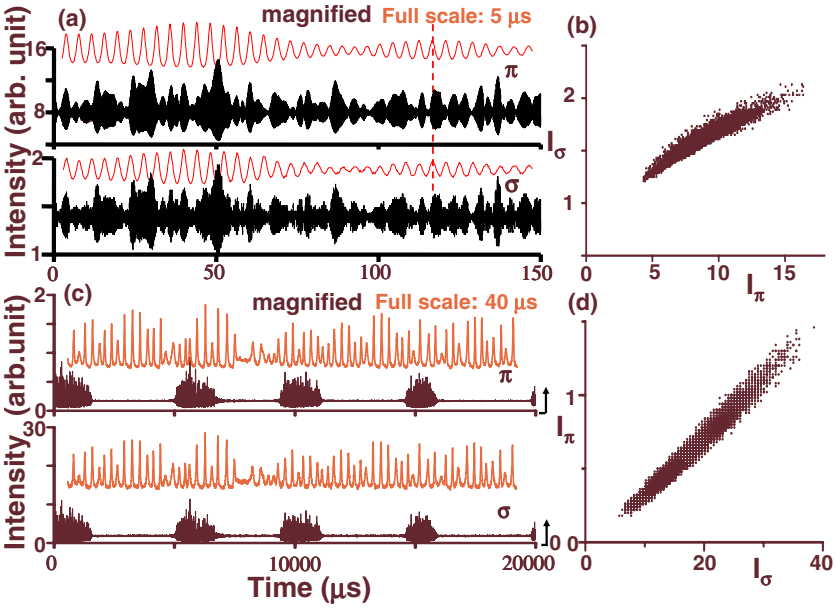


FIG. 4. (Color online) (a) Intensity wave forms and (b) correlation indicating in-phase synchronization of orthogonally polarized emissions in the case of self-mixing modulation. Pump power $P=447$ mW and modulation frequency $f_m=5.2$ MHz. The intensity correlation was fitted by $I_\sigma=0.07I_\pi-0.979$ with a standard deviation of 0.03. (c) Long-term temporal evolutions indicating synchronized random bursting and detailed modal intensity wave forms and (d) intensity correlation among orthogonally polarized emissions in the case of fiber feedback. Pump power $P=235$ mW. The intensity correlation was fitted by $I_\pi=0.038I_\sigma-0.069$ with a standard deviation of 0.03.

lasers [20], as will be shown in Sec. IV (see Fig. 11) and such synchronization never takes place in linearly polarized two mode lasers [18]. In other words, in the present dual-polarization laser, the dynamics of the $\pi$ mode, $I_\pi(t)$, was forced to reproduce the sum of two anticorrelated $\sigma$-mode dynamics, $I_\sigma(t)$. The observed phenomenon is a kind of chaos synchronization, in which two chaotic-spiking modes with anticorrelated intensity variations synchronize the remaining mode cooperatively with their total intensity variation. Chaotic nature of observed random time series of LS state and synchronized bursting has been identified by analyzing long-term experimental time series with the singular-value-decomposition (SVD) method [21].

In order to obtain further insight into such a chaos synchronization, we carried out a joint time-frequency analysis (JTFA) of the long-term time series [22]. Example time series of modal output intensities and the corresponding JTFA patterns are shown in Figs. 5 and 6, respectively. In the chaotic time domain, low-frequency fluctuation components indicated by the arrows in modal outputs, $I_{\sigma_1}(t)$ and $I_{\sigma_2}(t)$, which arose from the antiphase dynamics inherent in globally coupled multimode lasers [17], are suppressed in the total output, $I_\sigma(t)$ [18], indicating anticorrelated intensity variations of two $\sigma$ modes in the same polarization. The calculated JFTA patterns also indicate that the higher frequency fluctuation component of $I_\pi(t)$ predominantly reflects the chaotic motion of the $\sigma_1$ mode which mediates this switching event, as will be shown in Sec. IV.

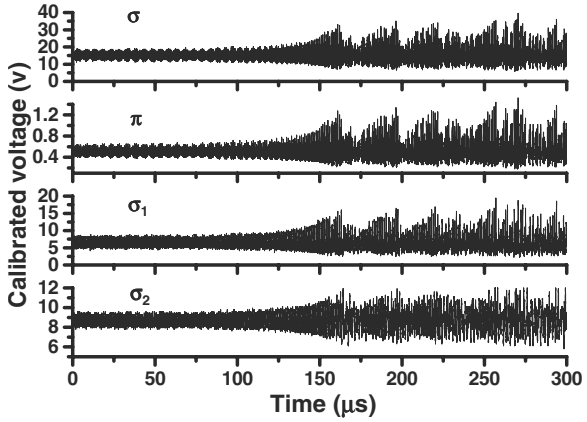


FIG. 5. Modal intensity variations indicating synchronization of bursting in the fiber feedback. $P=235$ mW.

### C. Numerical simulations

The model equations for lasers subjected to frequency-shifted optical feedback has been formulated in [23]. Under a short delay limit (i.e., delay time $\ll$ laser response time on the order of 1 $\mu$s), dynamics of the present dual-polarization la-

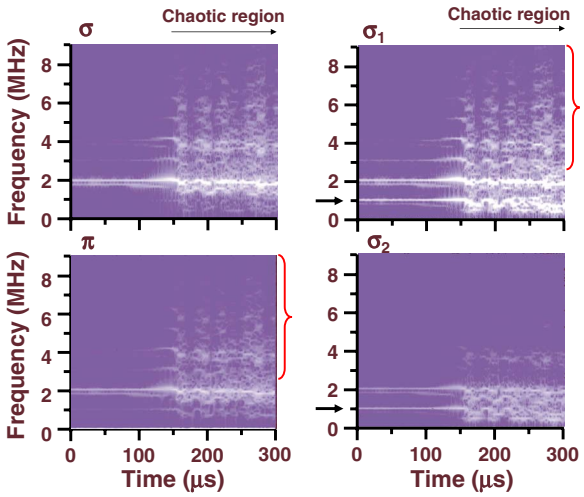


FIG. 6. (Color online) Joint time-frequency analysis of modal intensity variations shown in Fig. 5. Calculations were carried out using a moving window with a length of 2048 data points (40.96 $\mu$s) and a moving step with a length of 256 data points (5.12 $\mu$s).

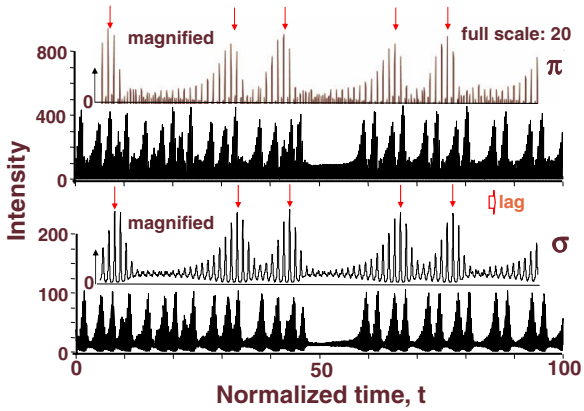


FIG. 7. (Color online) Numerical time series indicating an example lag synchronization. $W=6$, $g_1=1$, $g_2=0.19$, $g_3=0.20$, $\beta_{1,2}=\beta_{2,1}=0.387$, $\beta_{2,3}=\beta_{3,2}=0.528$, $\beta_{1,3}=\beta_{3,1}=0.329$. Modulation frequency was tuned to the relaxation oscillation, i.e., $\Omega_m=70.7$, with $m=0.085$ and $K=1000$.

ser can be treated by the following set of rate equations including the modulation term whose frequency is given by the Doppler-shift frequency in the self-mixing scheme [16,17,24].

$$dN_1/dt = W - g_1N_1(1 + S_1 + \beta_{1,2}S_2 + \beta_{1,3}S_3), \quad (1)$$

$$dN_2/dt = W - g_2N_2(1 + S_2 + \beta_{2,1}S_1 + \beta_{2,3}S_3), \quad (2)$$

$$dN_3/dt = W - g_3N_3(1 + S_3 + \beta_{3,1}S_1 + \beta_{3,2}S_2), \quad (3)$$

$$dS_1/dt = K(g_1N_1 - 1)S_1 + S_1m\cos\Omega_m t, \quad (4)$$

$$dS_2/dt = K(g_2N_2 - 1)S_2, \quad (5)$$

$$dS_3/dt = K(g_3N_3 - 1)S_3. \quad (6)$$

Here, $W$ is the pump power normalized by the threshold value of the first lasing mode, $N_i$ is the population density normalized by the threshold value of the first lasing mode, $S_i$ is the photon density normalized by that of the first lasing mode at $W=2$, $g_i$ is the gain ratio with respect to that of the first lasing mode, $K$ is the fluorescence-to-photon lifetime ratio, $\beta_{i,j}$ is the cross-saturation ratio, $m=2K\eta$ is the modulation index ($\eta$: field-amplitude feedback coefficient [16]), $\Omega_m=\omega_m\tau=2\pi(2v/\lambda)\tau$ is the normalized angular modulation frequency ($v$: moving speed of the cylinder along the laser axis), and time is normalized by the fluorescence lifetime, $\tau$. Mode numbers $i=1$, 2, and 3 correspond to the $\pi$, $\sigma_1$, and $\sigma_2$ modes, respectively.

Observed long-term amplitude envelope synchronizations and lag synchronizations have been reproduced qualitatively by numerical simulation of dual-polarization lasers subjected to self-mixing modulation, assuming relevant spectroscopic properties of $Nd:GdVO_4$ [14] and three-dimensional cross-saturation parameters among orthogonally polarized modes [15]. The numerical result indicating an example lag synchronization is shown in Fig. 7.

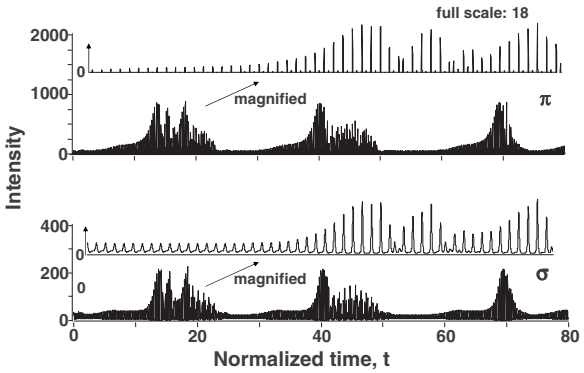


FIG. 8. Numerical result showing a synchronized random bursting. $W=6$, $g_1=1$, $g_2=0.19$, $g_3=0.20$, $\beta_{1,2}=\beta_{2,1}=0.387$, $\beta_{2,3}=\beta_{3,2}=0.528$, $\beta_{1,3}=\beta_{3,1}=0.329$, $\kappa_e=27$, $t_d=2\times10^4$, $\alpha=2$, and $K=1000$.

In the real experiment using self-mixing modulation by a Doppler-shifted optical feedback with the rotating cylinder, however, a reinjected light field possesses a narrow-band Gaussian frequency broadening on the order of several tens of kHz, which increases with a rotation speed of the cylinder [25]. Consequently, a Doppler-shift (i.e., modulation) frequency is not fixed in time unlike the simulation and the Gaussian-type of random process might influence the modulation term in Eq. (4) to some extent. It thus appears that chaotic spiking oscillations shown in Fig. 7 are smoothed in the real experiment. Such a stochastic effect on chaotic dynamics is under investigations.

On the other hand, the model equations for two-mode lasers coupled to a single-mode fiber have been already given in Eqs. (3)–(7) of Ref. [18], which include cross-saturation dynamics of population inversions among modes in the same form as Eqs. (1)–(3). By using model equations given in the Appendix, which were derived by extending Eqs. (3)–(7) of Ref. [18] to the present dual-polarization laser oscillating in three modes, we carried out numerical simulation. A typical numerical result is shown in Fig. 8. Here, uncorrelated Gaussian white noises are introduced into phase equations for $\sigma_1$ and $\sigma_2$ modes subjected to the common fiber feedback [18]. The observed synchronized random bursting among orthogonally polarized emissions are well reproduced.

## IV. INFORMATION CIRCULATION ANALYSIS OF OBSERVED SYNCHRONIZATION

In order to identify dynamic interplays among modes, we characterized the long-term modal intensity time series statistically with the information-theoretic quantity of information circulation among modes, $X$ and $Y$, defined as [18]: $T_{X,Y}=T_{X\to Y}-T_{Y\to X}$, $T_{X\to Y}=(1/\tau^*)\Sigma_\tau S(Y,Y_\tau|X) - (1/\tau^*)\Sigma_\tau S(Y,Y_\tau)$ is the information transfer rate from time series $X=x(t)$ to time series $Y=y(t)$, which is the self-mutual information for $Y$. Here, $S(Y,Y_\tau|X)$ is the conditional self-mutual information of time series $X$ given time series $Y$ and $\tau^*$ is the first local minimum of $S(Y,Y_\tau)$ [26]. The information circulation is derived from the original idea of transformation rate introduced by Palus *et al.*, which was success-

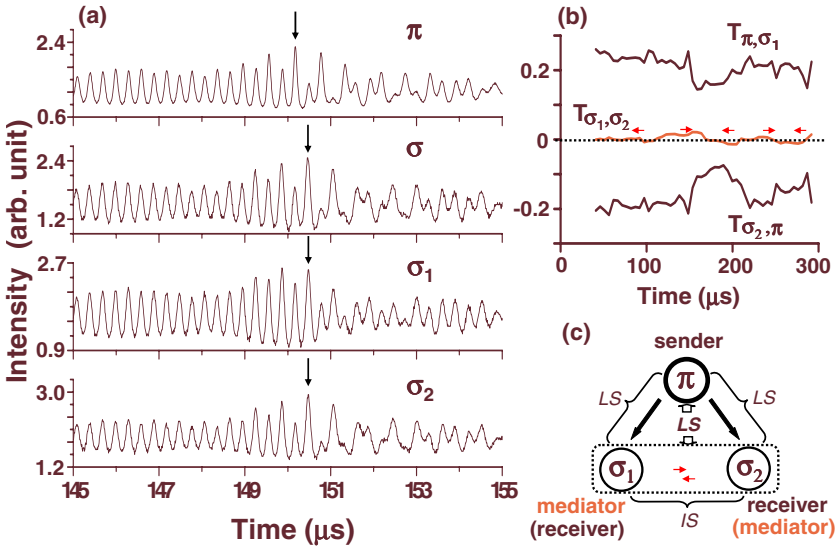


FIG. 9. (Color online) Information circulation analysis for lag synchronization states. $P=344$ mW. (a) Modal intensity wave forms, (b) calculated information circulations among three modes, and (c) information flow diagram, where the perturbed mode is indicated by a thick circle. The circulation analysis was carried out using the same data lengths as JTFA, where the light intensity was partitioned into 16 values to calculate intensity probability distributions.

fully used for characterizing organizations of brain tissues in terms of the direction of information flows [26]. Modal intensity variations (a) and the corresponding time-dependent information circulations (b), i.e., the net information flows, are summarized in Figs. 9–11, where the information flows from mode $i(j)$ to mode $j(i)$ if $T_{i,j}>0(<0)$. Here, information flow diagrams (c) are also depicted, where synchronization states among individual modes and orthogonally polarized emissions are depicted by "{" and "⇳," respectively.

As for the LS state, the $\pi$ mode subjected to self-mixing modulation acts as an information sender and sends a slightly different amount of information to $\sigma$ modes simultaneously, while nearly balanced bidirectional information flows take place among two $\sigma$ modes. To be more specific, the $\sigma_1(\sigma_2)$ mode behaves as an information mediator (receiver) and an information receiver (mediator) alternatively in time, as indicated by the arrows in Fig. 9(c). In the IS state, $\pi$ acts as a sender similar to the LS state and the $\sigma_2$ mode acts a receiver, while the $\sigma_1$ mode behaves as a mediator that receives information from the $\pi$ mode and transfers it to the $\sigma_2$ mode, as shown in Fig. 10(c).

Note that two $\sigma$ modes in the same polarization exhibit in-phase synchronizations, i.e., $I_{\sigma_2}=1.05I_{\sigma_1}+0.92$ (standard deviation=0.07) and $I_{\sigma_2}=4.16I_{\sigma_1}+1.17$ (standard deviation =0.06) for LS and IS, respectively. Here, for the correlation plot to identify synchronizations among modes in the same polarization, we used a time series with a length of 300 $\mu$s (i.e., $5\times10^4$ data points) for modal output whose relative intensity was accurately calibrated from the measured output-power ratio similarly to Figs. 3(c) and 4(b).

In the case of fiber feedback, the $\sigma_2$ mode serves as a sender, while the $\sigma_1$ mode acts as a mediator that receives information from the $\sigma_2$ mode, exhibiting antiphase dynamics, and transfers it to the $\pi$ receiver mode, as shown in Fig. 11(c). In short, the $\sigma_2$ mode among two perturbed modes is identified as triggering the simultaneous bursting for this particular time series (i.e., bursting event), as demonstrated in two-mode lasers subjected to common fiber feedback [18], and the nontrivial synchronization of $\pi$ mode to the superposition of two $\sigma$ modes is found to be established. Note that two perturbed $\sigma$ modes in the same polarization exhibit phase synchronization with anticorrelated intensity pulsa-

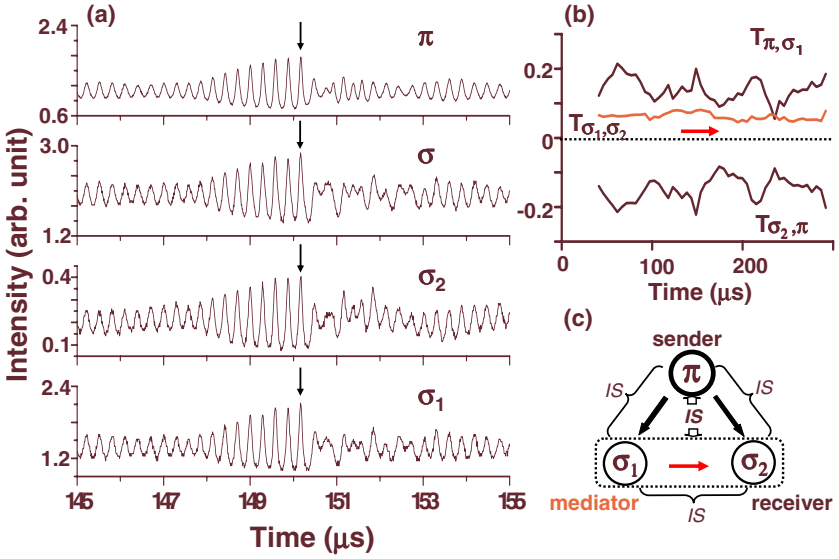


FIG. 10. (Color online) Information circulation analysis for in-phase synchronization states. $P=378$ mW. (a) Modal intensity wave forms, (b) calculated information circulations among three modes, and (c) information flow diagram, where the perturbed mode is indicated by a thick circle.

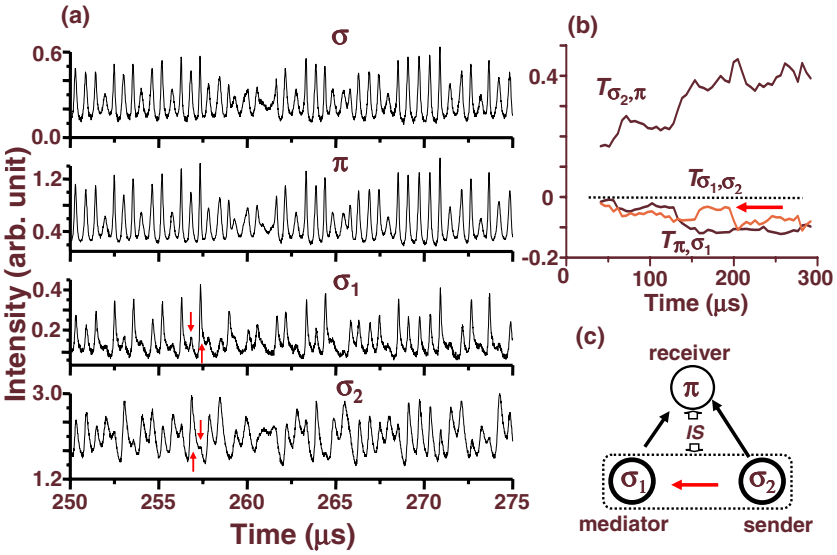


FIG. 11. (Color online) Information circulation analysis for cooperative synchronization of bursting. $P=235$ mW. (a) Modal intensity wave forms in the chaotic region of Fig. 5. (b) and (c) Information circulations and information flow diagram calculated from time series shown in Fig. 5, where the perturbed modes are indicated by a thick circle.

tions (i.e., antiphase dynamics) indicated by arrows, as mentioned in Sec. III B.

These information flow diagrams well characterize the dynamical roles of individual lasing modes in the crossed gain modulation scheme and provide reasonable physical insight into observed chaos synchronizations in the three-mode dual-polarization lasers.

Synchronization was not observed in the regime of two orthogonally polarized oscillations of the $\pi$ and $\sigma_2$ modes, i.e., pump power $P>500$ mW in Fig. 1. This implies that two-mode operations in the same polarization play a key dynamical role for chaos synchronizations of three interacting lasing modes. A clear understanding of the failure of chaos synchronization in two-mode lasers has yet to be achieved. However, a possible origin might be attributed to the large mismatch in physical parameters of two orthogonally polarized lasing modes, e.g., modal gain, loss, and intensity.

## V. CONCLUSION

In conclusion, we have investigated dynamic behaviors of an LD-pumped dual-polarization three-mode $Nd:GdVO_4$ laser subjected to external perturbations. The selective self-mixing modulation of one polarization mode resulted in in-phase synchronization of all lasing modes or lag synchronization among the perturbed mode and orthogonally polarized modes for decreased or increased cross saturation of population inversions among orthogonally polarized emissions, respectively. Synchronization of random bursting was found to take place when two modes in the same polarization were subjected to the common fiber feedback, in which two chaotic-spiking modes with anticorrelated intensity variations in one polarization cooperatively synchronize the remaining mode in the orthogonal polarization with their total intensity variation. The observed three types of synchronization were characterized by the information circulation analysis of long-term modal time series and dynamical roles of individual modes for establishing collective behaviors were identified.

The experimental observations and information-theoretic characterizations for the fundamental system size ($N=3$) demonstrated in the present paper will provide a basis for understanding chaos synchronizations in real-world complex systems with ensembles of many coupled elements. The observed chaos synchronizations could be observed in general dual-polarization lasers, e.g., VCSELs, in which rich collective dynamics are expected in $[m,n]$ schemes with many oscillating modes $m$ and $n$ in each polarization.

## APPENDIX: MODEL EQUATIONS OF DUAL-POLARIZATION LASERS SUBJECTED TO FIBER FEEDBACK

By introducing the common optical feedback to $\sigma_1$ and $\sigma_2$ modes from an optical fiber end surface and the cross saturation of population inversions among three lasing modes into Lang-Kobayashi equations [27], we obtain the following model equations:

$$dN_1/dt = W - g_1 N_1(1 + S_1 + \beta_{1,2} S_2 + \beta_{1,3} S_3), \quad \text{(A1)}$$

$$dN_2/dt = W - g_2 N_2(1 + S_2 + \beta_{2,1} S_1 + \beta_{2,3} S_3), \quad \text{(A2)}$$

$$dN_3/dt = W - g_3 N_3(1 + S_3 + \beta_{3,1} S_1 + \beta_{3,2} S_2), \quad \text{(A3)}$$

$$dS_1/dt = K(g_1 N_1 - 1)S_1, \quad \text{(A4)}$$

$$dS_2/dt = K(g_2 N_2 - 1)S_2 + 2\kappa_e \sqrt{S_2(t) S_2(t - t_d)} \cos \Theta_2(t), \quad \text{(A5)}$$

$$dS_3/dt = K(g_3 N_3 - 1)S_3 + 2\kappa_e \sqrt{S_3(t) S_3(t - t_d)} \cos \Theta_3(t), \quad \text{(A6)}$$

$$d\phi_2/dt = \Delta\Omega_2 + (1/2)\alpha K(g_2 N_2 - 1) - \kappa_e \sqrt{S_2(t - t_d)/S_2(t)} \sin \Theta_2(t) + F_{\phi,2}(t), \quad \text{(A7)}$$

$$d\phi_3/dt = \Delta\Omega_3 + (1/2)\alpha K(g_2 N_3 - 1) - \kappa_e \sqrt{S_3(t - t_d)/S_3(t)} \sin \Theta_3(t) + F_{\phi,3}(t), \quad \text{(A8)}$$

$$\Theta_2(t) = \Omega_2 t_d + \phi_2(t) - \phi_2(t - t_d), \tag{A9}$$

$$\Theta_3(t) = \Omega_3 t_d + \phi_3(t) - \phi_3(t - t_d). \tag{A10}$$

Here, we introduced uncorrelated modal lasing frequency fluctuations (i.e., phase noise), $F_{\phi,k}$ $(k=2,3)$, into phase equations for modes subjected to an optical feedback. $\phi_i$ is the slowly varying part of the optical phase of the lasing field $E_k \exp\{\omega_k t + \phi_k(t)\}$, and $\Theta_k$ is the phase difference between the lasing field and the reinjected field, $\Omega_k = \Omega_{0,k} + \Delta\Omega_k$, where $\Omega_k = \omega_k \tau$ is the normalized optical angular frequency of external cavity modes (ECMs) and $\Omega_{0,i} = \omega_{0,i}\tau$ is the normalized optical angular frequency of the $k$th solitary laser mode. $\alpha$ is the linewidth enhancement factor, which is nonzero in detuned lasers such as the present system, and the coupling strength is normalized as $\kappa_e = \kappa\tau$. Time $t$ and delay $t_d$ are normalized by the fluorescence lifetime, and other nomenclatures are the same as Eqs. (1)–(6). $F_{\phi,k}$ $(k=2,3)$ are uncorrelated Gaussian white noises that are $\delta$ correlated with zero mean.

The optical angular frequencies of ECMs are the solution of

$$\Delta\Omega_k t_d + C \sin(\Omega_k t_d + \tan^{-1}\alpha) = 0, \tag{A11}$$

where $C \equiv \kappa_e t_d \sqrt{1+\alpha^2}$. The steady-state characteristics can be characterized by $C$. In the case of $C<1$ as in the present experimental condition, there exists only one EMC in the vicinity of each solitary laser cavity frequency. Each ECM solution for $\sigma_k$ mode is not always stable depending on $\Delta\Omega_k t_d$ [27]. Therefore, the dynamical stability of ECM depends critically on the solitary laser cavity frequency $\Omega_{0,k}$ in a large delay case. If we consider frequency fluctuations (i.e., phase noise) resulting from a mode-partition-noise inherent in multimode lasers, each solitary laser cavity frequency, i.e., $\Delta\Omega_k$, fluctuates in time and a simultaneous random switching between stable and unstable states is expected to occur in time through cross saturation of population inversions [18].


[1] T. Sugawara, M. Tachikawa, T. Tsukamoto, and T. Shimizu, Phys. Rev. Lett. **72**, 3502 (1994).

[2] R. Roy and K. S. Thornburg, Jr., Phys. Rev. Lett. **72**, 2009 (1994).

[3] J. Ohtsubo, *Semiconductor Lasers: Stability, Instability and Chaos* (Springer-Verlag, Berlin, 2005).

[4] I. Fischer, R. Vicente, J. M. Buldu, M. Peil, C. R. Mirasso, M. C. Torrent, and J. Garcia-Ojalvo, Phys. Rev. Lett. **97**, 123902 (2006).

[5] E. Rodriguez, N. George, J.-P. Lachaux, J. Martinerie, B. Renaut, and F. J. Varela, Nature (London) **397**, 430 (1999).

[6] F. Rogister *et al.*, Opt. Lett. **26**, 1486 (2001).

[7] B. F. Kuntsevich and A. N. Pisarchik, Phys. Rev. E **64**, 046221 (2001).

[8] K. Otsuka and Y. Aizawa, Phys. Rev. Lett. **72**, 2701 (1994).

[9] K. Otsuka, Y. Sato, and J.-L. Chern, Phys. Rev. A **54**, 4464 (1996).

[10] K. Otsuka, Y. Sato, and J.-L. Chern, Phys. Rev. E **56**, 4765 (1997).

[11] Y. Hong *et al.*, Opt. Lett. **29**, 2151 (2004).

[12] A. Gavrielides *et al.*, Opt. Lett. **31**, 2006 (2006).

[13] R. Ju *et al.*, IEEE J. Quantum Electron. **QE-41**, 1461 (2005).

[14] F. G. Anderson, P. L. Summers, H. Weidner, P. Hong, and R. E. Peale, Phys. Rev. B **50**, 14802 (1994); Y. Sato and T. Taira, IEEE J. Quantum Electron. **11**, 613 (2005).

[15] J.-Y. Ko *et al.*, Opt. Express **15**, 945 (2007).

[16] K. Otsuka, IEEE J. Quantum Electron. **QE-15**, 655 (1979); R. Kawai, Y. Asakawa, and K. Otsuka, IEEE Photonics Technol. Lett. **11**, 706 (1999).

[17] See, for example: K. Otsuka, *Nonlinear Dynamics in Optical Complex Systems* (Springer-Verlag, Berlin, 2000).

[18] K. Otsuka, J.-Y. Ko, T. Ohtomo, and K. Ohki, Phys. Rev. E **64**, 056239 (2001).

[19] D. Gabor, J. Inst. Electr. Eng., Part 3 **93**, 429 (1946).

[20] R. Meucci, F. Salvadori, M. V. Ivanchenko, K. A. Naimee, C. Zhou, F. T. Arecchi, S. Boccaletti, and J. Kurths, Phys. Rev. E **74**, 066207 (2006).

[21] K. Otsuka, J. Y. Ko, J. L. Chern, K. Ohki, and H. Utsu, Phys. Rev. A **60**, R3389 (1999).

[22] K. Otsuka *et al.*, Chaos **13**, 1014 (2003).

[23] J.-Y. Ko, K. Otsuka, and T. Kubota, Phys. Rev. Lett. **86**, 4025 (2001).

[24] Y. Miyasaka, K. Otsuka, T. Maniwa, and J. Y. Ko, Phys. Rev. E **70**, 046208 (2004).

[25] F. T. Arecchi, "Photocount distributions and field statistics," in *Quantum Optics*, edited by R. J. Glauber (Academic Press, New York, 1969).

[26] M. Palus, Physica D **93**, 64 (1996); M. Palus, V. Komarek, Z. Hrncir, and K. Sterbova, Phys. Rev. E **63**, 046211 (2001).

[27] R. Lang and K. Kobayashi, IEEE J. Quantum Electron. **QE-16**, 347 (1980).